

Complexity and Operator Growth in Holographic 6d SCFTs

Ali Fatemiabhari^{a,b} Carlos Nunez^a and Ricardo T. Santamaria^a

^a*Centre for Quantum Fields and Gravity, Department of Physics, Swansea University, Swansea SA2 8PP, United Kingdom*

^b*Institute for Theoretical and Mathematical Physics, Lomonosov Moscow State University, 119991 Moscow, Russia*

ABSTRACT: We study Krylov (spread) complexity in strongly coupled six-dimensional $\mathcal{N} = (1, 0)$ superconformal field theories with holographic duals in massive type IIA supergravity. Extending recent holographic proposals relating Krylov complexity growth to the proper momentum of an infalling particle, we analyse the dynamics of massive geodesic probes in these geometries. In our setup, the bulk particle is allowed to move along three directions: the radial AdS coordinate, the internal S^2 associated with the $SU(2)_R$ symmetry, and the coordinate parametrising the quiver. In the dual field theory these motions encode, respectively, operator growth, the presence of R-symmetry charges, and spreading across different nodes of the quiver. We analyse the geodesic motion both analytically and numerically for representative quiver configurations. The motion along the quiver direction is typically damped and localised at early times, while the late-time behaviour is dominated by the radial AdS motion. As a consequence, the generalised proper momentum grows linearly at late times, consistent with expectations for Krylov complexity in conformal theories. The inclusion of angular momentum ($SU(2)_R$ charge) introduces additional constraints on the allowed motion and modifies the early-time dynamics while leaving the asymptotic behaviour unchanged. These results provide a first exploration of Krylov complexity in higher-dimensional holographic conformal theories and reveal how operator growth can probe both internal symmetries and quiver structure in strongly coupled conformal field theories.

Contents

1	Introduction and General Idea	1
2	Super Conformal Theories in Six Dimensions and Holographic Dual	3
2.1	Two examples	6
2.1.1	<u>Quiver 1</u>	6
2.1.2	<u>Quiver 2</u>	6
3	Krylov (Spread) Complexity	7
3.1	A general geodesic	9
3.2	Generalised proper momentum	10
3.3	Geodesics with $J = 0$	12
3.3.1	Quiver 1	12
3.3.2	Quiver 2	13
3.4	Geodesics with $J \neq 0$	15
3.4.1	Quiver 1	17
3.4.2	Quiver 2	18
4	Discussion, Further Comments and Conclusions	19

1 Introduction and General Idea

Understanding how quantum information spreads in strongly interacting quantum systems has become a central theme connecting quantum field theory, quantum information and gravitational physics. In recent years, ideas from quantum complexity have proven particularly useful in characterising the growth of operators, thermalisation and chaotic dynamics in many-body systems. For recent review articles, see [1–3].

In holography [4], where strongly coupled dynamics can be described geometrically, these ideas have led to a fruitful interplay between gravitational physics and quantum information. In the context of gauge/gravity duality, several proposals relate the complexity of quantum states in the boundary field theory to geometric quantities in the dual gravitational description.

These ideas have motivated an extensive literature studying complexity in holography and quantum field theory. Recently, Krylov complexity has emerged as a particularly natural measure of operator growth in quantum many-body systems [5]. In this framework one constructs the Krylov basis generated by repeated action of the Hamiltonian on a given state or operator. The resulting Lanczos coefficients determine an effective one-dimensional chain describing the evolution of the system, and the spread of the wavefunction along this

chain defines the Krylov complexity [5, 6]. These ideas have been explored in a variety of systems including conformal field theories and holographic models [7–10].

A particularly interesting holographic proposal was put forward in [11], where the growth rate of Krylov complexity in holographic two-dimensional conformal field theories was related to the proper radial momentum of a falling particle in the dual bulk geometry. In this picture, operator growth in the boundary theory is mapped to the motion of particles following geodesics in the gravitational background. This proposal provides an appealing geometric description of operator spreading and raises the question of how such ideas extend to more general holographic systems, particularly to higher dimensional strongly coupled quantum field theories.

Six-dimensional $\mathcal{N} = (1, 0)$ superconformal field theories provide a particularly interesting setting to explore these questions. These theories arise in string theory through Hanany-Witten [12] type brane constructions involving NS5, D6 and D8 branes [13, 14]. Although many of these theories do not admit a conventional Lagrangian description, they possess well understood holographic duals in massive type IIA supergravity in terms of AdS_7 backgrounds [15–18]. The geometry of these solutions is characterised by a function $\alpha(\eta)$ whose derivatives encode the rank function of a linear quiver describing the tensor branch of the theory [15]. These systems therefore provide a rich framework in which strongly coupled dynamics, brane physics and holography can be studied simultaneously. The entanglement entropy in field theories dual to these backgrounds and their deformations are studied in [19].

In this paper we investigate Krylov complexity in the context of these six-dimensional holographic theories. Extending the proposal of [11, 20], we model the spreading of operators in the SCFT by the motion of a massive particle following a timelike geodesic in the dual AdS_7 background. In this construction, motion along the internal S^2 directions encodes the $SU(2)_R$ charge of the operator, which is analogous to symmetry resolved Krylov complexity [21, 22]). Similarly, motion along the coordinate η corresponds to spreading across different nodes of the quiver [20]. We derive the corresponding equations of motion and analyse them both analytically and numerically for two representative quiver configurations. Our results show that the motion along the quiver direction is typically damped and largely confined to early times, while at late times the dynamics is dominated by the radial motion in AdS . Consequently, the generalised proper momentum, which we interpret as the rate of holographic complexity growth, approaches a linear behaviour at late times, consistent with expectations for conformal theories.

The rest of the paper is organised as follows. In Section 2 we review the holographic description of six-dimensional $\mathcal{N} = (1, 0)$ SCFTs and introduce the two quiver examples that we will use throughout the paper. In Section 3 we review Krylov complexity and extend the holographic prescription relating complexity growth to generalised proper momentum in the bulk. We then analyse the resulting geodesic equations for different quiver configurations and values of the R -symmetry charge, we draw some parallels with symmetry resolved Krylov complexity. A careful numeric study is presented in detail. In Section 4 we summarise our results and discuss several directions for future work.

2 Super Conformal Theories in Six Dimensions and Holographic Dual

Let us start with a short summary of six-dimensional $\mathcal{N} = (1, 0)$ conformal field theories and their holographic description. It is useful to recall the main obstruction for interacting local quantum field theories in dimensions $d > 4$. Consider a simple scalar field theory in six dimensions,

$$S = \int d^6x \left[-\frac{1}{2}(\partial_\mu\phi)^2 - V(\phi) \right].$$

A real scalar has classical mass-dimension $[\phi] = m^2$, a mass term reads $V = \frac{m^2}{2}\phi^2$. A marginal-looking cubic $V = g\phi^3$ is problematic as it lacks a bounded below potential for $\phi < 0$, while a stable $\lambda\phi^4$ interaction is irrelevant in six dimensions, so the theory requires a UV completion. The Wilsonian intuition (start with a UV CFT and perturb by relevant operators) appears not to straightforwardly supply interacting renormalisable models in $d = 6$.

Despite this, string constructions indicate that supersymmetric theories of scalars coupled to gauge fields may possess interacting UV fixed points. For example, a schematic Lagrangian

$$\mathcal{L} \sim -\frac{1}{2}(\partial_\mu\phi)^2 - c\phi F_{\mu\nu}^2 + \text{fermions}, \quad (2.1)$$

shows that when $\langle\phi\rangle \rightarrow 0$ one probes the strong coupling limit of a gauge theory, with ϕ playing the role of the inverse gauge coupling. Supersymmetry introduces fermions and potential gauge anomalies; anomaly cancellation is possible when ϕ sits in a tensor multiplet [23, 24], with a finely tuned matter content.

Hanany–Witten type brane constructions realise such theories, see [12, 13]. The six-dimensional $\mathcal{N} = (1, 0)$ theories preserve eight Poincaré supercharges and have bosonic symmetry $SO(1, 5) \times SU(2)_R$. The relevant multiplets are:

- **Tensor multiplet:** $(B_{\mu\nu}, \lambda_1, \lambda_2, \phi)$ (self-dual two-form, fermions, real scalar).
- **Vector multiplet:** $(A_\mu, \hat{\lambda}_1, \hat{\lambda}_2)$.
- **Hypermultiplet:** $(\varphi_1, \varphi_2, \psi_1, \psi_2)$.
- **Linear multiplet:** $(\vec{\pi}, c, \tilde{\xi})$ (an $SU(2)$ triplet, singlet and a fermion).

When the tensor scalar acquires a VEV (the *tensor branch*) the $SU(2)_R$ symmetry is preserved. VEVs of hyper/linear multiplets explore the Higgs branch, breaking $SU(2)_R$. In this paper, we focus on the tensor branch.

To realise these theories from branes one distributes NS5, D6 and D8 branes as in Table 1.

Important differences with lower-dimension Hanany–Witten systems include: the NS5 and bounded D6 worldvolumes have the same dimension so five-brane dynamics do not decouple and tensor multiplets (provided by the NS branes) appear. These tensor multiplets are needed to cancel a gauge anomaly [13]. The brane content (analogously, the stability of the brane set-up) is restricted to satisfy

$$N_{D6,R} + N_{D6,L} + N_{D8} = 2N_{D6,c}, \quad (2.2)$$

	t	x_1	x_2	x_3	x_4	x_5	x_6	x_7	x_8	x_9
NS5	•	•	•	•	•	•	•	•	•	•
D6	•	•	•	•	•	•	•	•	•	•
D8	•	•	•	•	•	•	•	•	•	•

Table 1. Brane set-up: all branes extend on Minkowski $\mathbb{R}^{1,5}$. D6's are finite along x_6 between NS5's; D8's extend along $x_{7,8,9}$ preserving $SO(3)_R$.

where $N_{D6,R/L}$ are sixbranes to the right/left of a 'colour' stack of $N_{D6,c}$ branes. D2-branes on (t, x_1, x_6) ending on NS5's represent strings charged under the self-dual H_3 . These strings have a dual role. They are coupled to the tensor multiplets living on the world-volume of the NS-branes and are thus charged both electrically and magnetically to the tensor multiplet. In addition, they are instantons to the gauge fields living on the D6-branes.

Flowing to the IR, when the tensor-branch separations are taken as $\langle \phi_i - \phi_{i-1} \rangle \neq 0$, these instantonic strings become massive and the low-energy theory admits an anomaly-free quiver description. On the other hand, in the tensionless string limit $\langle \phi_i - \phi_{i-1} \rangle \rightarrow 0$ the system is proposed to be UV-completed by a strongly coupled 6d CFT [23]. These fixed points have a holographic description that we discuss now.

Massive Type IIA duals: AdS₇ backgrounds and the quiver map

We now summarise the massive Type IIA supergravity backgrounds dual to these $\mathcal{N} = (1, 0)$ SCFTs. The family of solutions was written in [16, 17]; we follow the notation of [25]. The backgrounds (metric, NS B_2 , dilaton Φ , RR fields F_0, F_2) possess $SO(2, 6) \times SU(2)_R$ isometries and, in *Einstein frame*¹ take the form

$$\begin{aligned}
ds_E^2 &= f_1(\eta) ds_{AdS_7}^2 + f_2(\eta) d\eta^2 + f_3(\eta) d\Omega_2(\theta, \varphi), \\
B_2 &= f_4(\eta) \text{Vol}(S^2), \quad F_2 = f_5(\eta) \text{Vol}(S^2), \quad e^\Phi = f_6(\eta), \\
ds^2(\text{AdS}_7) &= dr^2 + e^{-2r} (dx_{1,5}^2), \quad d\Omega_2 = d\theta^2 + \sin^2 \theta d\varphi^2, \quad \text{Vol}(S^2) = \sin \theta d\theta \wedge d\varphi.
\end{aligned} \tag{2.3}$$

The functions $f_i(\eta)$ are expressed in terms of a single function $\alpha(\eta)$ and its derivatives,

$$\begin{aligned}
f_1(\eta) &= 8\sqrt{2}\pi e^{-\frac{\Phi}{2}} \sqrt{-\frac{\alpha}{\alpha''}}, \quad f_2(\eta) = \sqrt{2}\pi e^{-\frac{\Phi}{2}} \sqrt{-\frac{\alpha''}{\alpha}}, \\
f_3(\eta) &= \sqrt{2}\pi e^{-\frac{\Phi}{2}} \sqrt{-\frac{\alpha''}{\alpha}} \left(\frac{\alpha^2}{(\alpha')^2 - 2\alpha\alpha''} \right), \\
f_4(\eta) &= \pi \left(-\eta + \frac{\alpha\alpha'}{(\alpha')^2 - 2\alpha\alpha''} \right), \quad f_5(\eta) = \left(\frac{\alpha''}{162\pi^2} + \frac{\pi F_0 \alpha \alpha'}{(\alpha')^2 - 2\alpha\alpha''} \right), \\
f_6(\eta) &= 2^{5/4} \pi^{5/2} 3^4 \frac{(-\alpha/\alpha'')^{3/4}}{\sqrt{(\alpha')^2 - 2\alpha\alpha''}}.
\end{aligned} \tag{2.4}$$

¹This choice of frame is motivated by the fact that we probe this background with particles, which couple to the Einstein frame metric.

Supersymmetry and the massive IIA equations require $\alpha(\eta)$ to satisfy

$$\alpha'''(\eta) = -162\pi^3 F_0, \quad (2.5)$$

so for piecewise-constant Romans mass F_0 one finds $\alpha(\eta)$ as piecewise cubic,

$$\alpha(\eta) = a_0 + a_1\eta + \frac{a_2}{2}\eta^2 - \frac{162\pi^3 F_0}{6}\eta^3. \quad (2.6)$$

Cremonesi and Tomasiello [25] gave a practical recipe mapping balanced linear quivers to an $\alpha(\eta)$ solving eq.(2.5). Introduce the (piecewise-linear) rank function

$$R(\eta) = -\frac{1}{81\pi^2}\alpha''(\eta), \quad (2.7)$$

and consider a linear quiver with P gauge nodes such that

$$R(\eta) = \begin{cases} N_1\eta & 0 \leq \eta \leq 1, \\ N_1 + (N_2 - N_1)(\eta - 1) & 1 \leq \eta \leq 2, \\ \vdots & \\ N_P(P + 1 - \eta) & P \leq \eta \leq P + 1. \end{cases}$$

The ranks of the gauge groups are encoded in R evaluated at integers $\eta = 1, \dots, P$, and the balancing condition reads

$$R''(\eta) = \sum_{k=1}^P F_k \delta(\eta - k), \quad F_k = 2N_k - N_{k-1} - N_{k+1}, \quad (2.8)$$

so that each F_k gives the number of flavours coupled to node k . Given $R(\eta)$ one integrates $-81\pi^2 R(\eta)$ twice to obtain $\alpha(\eta)$, fixing integration constants by continuity of α, α' and imposing $\alpha(0) = \alpha(P) = 0$.

When this $\alpha(\eta)$ is plugged into (2.3)–(2.4) the resulting geometry is the holographic dual to the UV SCFT₆ associated to the quiver of Figure 1 (evaluated at the origin of the tensor branch).

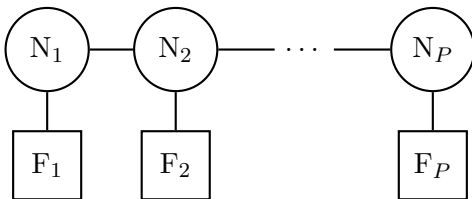


Figure 1. Linear quiver: balancing implies $F_k = 2N_k - N_{k-1} - N_{k+1}$.

Several holographic tests have been performed: Page charges for RR/NS fields map to the quiver and Hanany–Witten brane picture; holographic free energy computations can be compared with field theory expressions [26]; see [27, 28] for further observables computed holographically.

2.1 Two examples

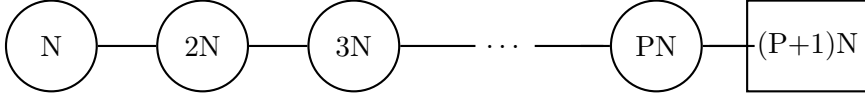
We discuss two examples of the previous formalism. These are used below to evaluate our expression for complexity derived in later sections.

2.1.1 Quiver 1

For the first case, we chose a quiver that features a flavour group at $\eta = P$, resulting in $\alpha(\eta)$ and a triangular rank function.

$$R_1(\eta) = -\frac{1}{81\pi^2}\alpha_1''(\eta) = \begin{cases} N\eta & 0 \leq \eta \leq P, \\ NP(P+1-\eta) & P \leq \eta \leq P+1; \end{cases}$$

the corresponding quiver is



The function $\alpha_1(\eta)$ reads,

$$\alpha_1(\eta) = -81\pi^2 N \begin{cases} a_1\eta + \frac{1}{6}\eta^3 & 0 \leq \eta \leq P \\ (Pa_1 + \frac{P^3}{6}) + (a_1 + \frac{P^2}{2})(\eta - P) + \frac{P}{2}(\eta - P)^2 - \frac{P}{6}(\eta - P)^3 & P \leq \eta \leq P+1. \end{cases} \quad (2.9)$$

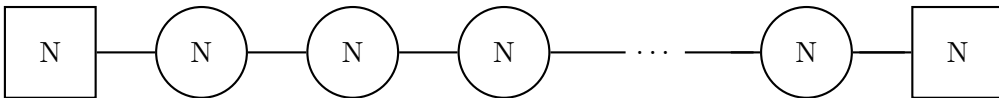
Where $k := 1, \dots, P-1$ and $a_1 = -\frac{P(P+2)}{6}$. One can check that $\alpha_1(\eta)$ and $\alpha_1'(\eta)$ are continuous and $\alpha_1''(\eta) = -81\pi^2 R_1(\eta)$.

2.1.2 Quiver 2

Here, we choose a quiver with two flavour groups, one at $\eta = 1$ and one at $\eta = P$. The rank function is,

$$R_2(\eta) = -\frac{1}{81\pi^2}\alpha_2''(\eta) = \begin{cases} N\eta & 0 \leq \eta \leq 1, \\ N & 1 \leq \eta \leq P; \\ N(P+1-\eta) & P \leq \eta \leq P+1; \end{cases}$$

the corresponding quiver is



The function $\alpha_2(\eta)$ is

$$-\frac{\alpha_2(\eta)}{81\pi^2 N} = \begin{cases} a_1\eta + \frac{\eta^3}{6} & 0 \leq \eta \leq 1 \\ \left(a_1 + \frac{1}{6}\right) + \left(a_1 + \frac{1}{2}\right)(\eta - 1) + \frac{1}{2}(\eta - 1)^2 & 1 \leq \eta \leq 2 \\ \left(2a_1 + \frac{7}{6}\right) + \left(a_1 + \frac{3}{2}\right)(\eta - 2) + \frac{1}{2}(\eta - 2)^2 & 2 \leq \eta \leq 3 \\ \left(3a_1 + \frac{19}{6}\right) + \left(a_1 + \frac{5}{2}\right)(\eta - 3) + \frac{1}{2}(\eta - 3)^2 & 3 \leq \eta \leq 4 \\ \dots \\ \left(ka_1 + \frac{3k^2 - 3k + 1}{6}\right) + \left(a_1 + \frac{2k - 1}{2}\right)(\eta - k) + \frac{1}{2}(\eta - k)^2, & k \leq \eta \leq k + 1 \\ \left(Pa_1 + \frac{3P^2 - 3P + 1}{6}\right) + \left(a_1 + \frac{2P - 1}{2}\right)(\eta - P) + \frac{1}{2}(\eta - P)^2 - \frac{1}{6}(\eta - P)^3, & P \leq \eta \leq P + 1, \end{cases} \quad (2.10)$$

Here $a_1 = -\frac{P}{2}$ and $1 \leq k \leq P - 1$.

As a summary, we have presented the holographic description of six dimensional $\mathcal{N} = (1, 0)$ SCFTs linear quivers. Papers studying further aspects of these SCFTs are [16, 17, 29–40]. We have quoted the function $\alpha(\eta)$ and its second derivative (the rank function), for two special quivers that are generic enough and easy to work with. We use these quivers in the remainder of the paper, when we study specific numerics. Let us now focus on the Krylov (spread) complexity.

3 Krylov (Spread) Complexity

In this section, we start with a short introduction to Krylov/spread complexity and the calculation of [11]. Then, we generalise this calculation to the six dimensional SCFTs of linear quiver type discussed above. We follow the work of [20].

Given a Hamiltonian H and an initial state $|\psi_0\rangle$, the Krylov subspace $\mathcal{K} = \text{span}\{|\psi_0\rangle, H|\psi_0\rangle, H^2|\psi_0\rangle, \dots\}$ admits an orthonormal Krylov/Lanczos basis $\{|n\rangle\}_{n \geq 0}$ constructed by the Lanczos algorithm. Expanding the evolved state as

$$|\psi(t)\rangle = e^{-iHt}|\psi_0\rangle = \sum_{n \geq 0} \phi_n(t) |n\rangle. \quad (3.1)$$

We have $\sum_n |\phi_n(t)|^2 = 1$, and the amplitudes obey a discrete Schrödinger equation on an effective 1D chain,

$$i\dot{\phi}_n(t) = a_n \phi_n(t) + b_{n+1} \phi_{n+1}(t) + b_n \phi_{n-1}(t), \quad b_0 := 0, \quad (3.2)$$

where $\{a_n, b_n\}$ are the (real) Lanczos coefficients. The spread complexity (a state-version of Krylov complexity) is the average position on this chain,

$$\mathcal{C}(t) \equiv \sum_{n \geq 0} n |\phi_n(t)|^2 \quad \left(\text{with } p_n(t) := |\phi_n(t)|^2\right). \quad (3.3)$$

Operationally one does the following: first, compute the return amplitude $\langle \psi_0 | \psi(t) \rangle$. Then, extract the moments to obtain $\{a_n, b_n\}$. Finally, solve for $\phi_n(t)$, and then evaluate $\mathcal{C}(t)$.

The holographic set-up of [11] can be described as follows. The authors of [11] study locally excited states in holographic 2D CFTs, prepared by inserting a primary operator \mathcal{O} (with a small Euclidean smearing) into a thermal (TFD) or vacuum background. Conformal symmetry fixes the relevant return amplitudes in terms of ratios of two-point functions, which in turn leads to analytic Lanczos data and hence to closed-form expressions for the rate $\dot{\mathcal{C}}(t)$ in these 2D CFT examples. The key Physics is that after a characteristic time scale, $\dot{\mathcal{C}}(t)$ captures the expected rapid growth associated with operator/state spreading in a holographic theory [11].

The proposal of [11]—see also [41, 42] for elaborations and refinements, is to calculate the time derivative of the complexity rate as *proper* radial momentum. On the gravity side, the same local excitation is semi-classically approximated by a massive particle falling along a timelike radial geodesic in an asymptotically AdS₃ geometry (vacuum, global AdS, or BTZ, depending on the CFT state). The authors of [11] propose to use the radial coordinate ρ measuring *proper radial distance* (e.g. to the horizon in BTZ, or to the Poincaré “horizon” in vacuum AdS). Writing the relevant 2D (t, ρ) part of the metric as

$$ds_{(2)}^2 = -f(\rho) dt^2 + d\rho^2, \quad (3.4)$$

the *proper momentum* is the momentum conjugate to ρ along the worldline,

$$P_\rho \equiv \frac{\partial L}{\partial \dot{\rho}} \quad (\text{with } L = -m\sqrt{-g_{\mu\nu}\dot{x}^\mu\dot{x}^\nu}). \quad (3.5)$$

The holographic dictionary entry proposed and verified in their AdS₃/CFT₂ examples is

$$\boxed{\dot{\mathcal{C}}(t) \sim P_\rho(t)} \quad (3.6)$$

(up to the normalization conventions).

In summary, the procedure is this: first, compute $\dot{\mathcal{C}}(t)$ from CFT correlators via the Krylov chain. Second, calculate $P_\rho(t)$ from the infalling geodesic in proper-distance gauge and finally match them.

In what follows, we apply this logic for our AdS₇ system. It is important that in our case, the strongly coupled system is not described in terms of a quiver field theory. The best (and only) description is in terms of the holographic background in eq.(2.3). The application of the recipe of [11] to our case is not accompanied by a CFT calculation, though the ingredients are present. We allow the massive particle to move along the AdS-radial coordinate, the $S^2(\theta, \varphi)$ directions and the quiver η -direction. In this way the massive particle falling along a geodesic represents the time evolution of an operator of the CFT₆. This operator has SU(2) R-charge (enacted by the motion on S^2), and spreads along the different nodes in the quiver, represented by the motion along η -coordinate. The treatment is reminiscent of that in [20], with the added subtlety of the R-symmetry quantum numbers.

Let us start studying a generic geodesic.

3.1 A general geodesic

We consider a time-like geodesic on the family of backgrounds described by eqs.(2.3)-(2.6). The geodesics is parametrised by the t -coordinate. We propose the following (consistent) embedding,

$$r(t), \quad \theta(t) = \frac{\pi}{2}, \quad \varphi(t), \quad \eta(t). \quad (3.7)$$

The induced metric along the geodesic is

$$ds_{ind,E}^2 = \left[f_1(\eta) \left(-e^{-2r} + \dot{r}^2 \right) + f_2(\eta) \dot{\eta}^2 + f_3(\eta) \dot{\varphi}^2 \right] dt^2, \quad (3.8)$$

and the action associated with this particle is

$$S = -m \int dt \sqrt{f_1(\eta) (e^{-2r} - \dot{r}^2) - f_2(\eta) \dot{\eta}^2 - f_3(\eta) \dot{\varphi}^2}. \quad (3.9)$$

We also define

$$L = \sqrt{f_1(\eta) (e^{-2r} - \dot{r}^2) - f_2(\eta) \dot{\eta}^2 - f_3(\eta) \dot{\varphi}^2}, \quad (3.10)$$

that leads to the following equations of motion,

$$\frac{d}{dt} \left(\frac{f_1(\eta)}{L} \dot{r} \right) = \frac{f_1(\eta)}{L} e^{-2r}, \quad (3.11)$$

$$\frac{d}{dt} \left(\frac{f_2(\eta)}{L} \dot{\eta} \right) = -\frac{1}{2L} \left[f_1'(\eta) (e^{-2r} - \dot{r}^2) - f_2'(\eta) \dot{\eta}^2 - f_3'(\eta) \dot{\varphi}^2 \right], \quad (3.12)$$

$$\frac{d}{dt} \left[\frac{f_3(\eta)}{L} \dot{\varphi} \right] = 0. \quad (3.13)$$

We have two conserved quantities in this system. One is the Hamiltonian, given by

$$H = \frac{mf_1(\eta)e^{-2r}}{\sqrt{f_1(\eta) (e^{-2r} - \dot{r}^2) - f_2(\eta) \dot{\eta}^2 - f_3(\eta) \dot{\varphi}^2}}. \quad (3.14)$$

The second conserved quantity is the angular momentum J , from eq.(3.13)

$$J = \frac{f_3(\eta)}{L} \dot{\varphi}. \quad (3.15)$$

Using the Hamiltonian in eq.(3.14) and the angular momentum in eq.(3.15) we solve for $\dot{\eta}$ and $\dot{\varphi}$,

$$\dot{\varphi} = \frac{mJ}{H} \frac{f_1(\eta)}{f_3(\eta)} e^{-2r(t)}, \quad (3.16)$$

$$\dot{\eta} = \pm \frac{e^{-2r(t)}}{H} \sqrt{\frac{f_1(\eta)}{f_2(\eta)f_3(\eta)}} \times \sqrt{e^{2r(t)} H^2 f_3(\eta) - m^2 f_1(\eta) (J^2 + f_3(\eta)) - H^2 e^{4r(t)} f_3(\eta) \dot{r}^2}.$$

Taking derivatives of these and replacing them in eqs.(3.11)-(3.13), one finds that all equations of motion are satisfied if,

$$e^{2r(t)} \ddot{r} + 2e^{2r(t)} \dot{r}^2 - 1 = 0. \quad (3.17)$$

We consider the function $r(t)$ satisfying $r(0) = r_{UV}$, $\dot{r}(0) = 0$, namely a particle that falls from the position r_{UV} with zero initial velocity,

$$r(t) = \frac{1}{2} \log \left(e^{2r_{UV}} + t^2 \right). \quad (3.18)$$

Replacing this in the expressions in eq.(3.16), we find

$$\begin{aligned} \dot{\varphi} &= \frac{J}{H} \frac{f_1(\eta)}{f_3(\eta)} \left(\frac{1}{t^2 + e^{2r_{UV}}} \right), \\ \dot{\eta} &= \pm \frac{1}{H} \left(\frac{1}{e^{2r_{UV}} + t^2} \right) \sqrt{\frac{f_1(\eta)}{f_2(\eta)f_3(\eta)} [H^2 e^{2r_{UV}} f_3(\eta) - m^2 f_1(\eta)(J^2 + f_3(\eta))]} \end{aligned} \quad (3.19)$$

The problem to be solved is the following: given a 6d $\mathcal{N} = (1, 0)$ SCFT characterised by a function $\alpha(\eta)$ —and its dual background described by the functions $f_i(\eta)$ in eq.(2.4)—we need to solve for $\eta(t), \varphi(t)$ in eqs.(3.19). The solutions to these equations describe the geodesic in eq.(3.7), for the holographic dual background to a particular $\mathcal{N} = (1, 0)$ superconformal field theory of the quiver type. In terms of the SCFT, an operator with a given conformal dimension and R-charge spreads into other operators with the same R-charge (motion in φ with conserved J) and into operators that connect with different nodes of the quiver (this is allowed by the presence of bifundamental fields). The motion along the radial coordinate, described by eqs.(3.17),(3.18) is the same as in [11] and reminds us that the evolution/spread is constrained by conformal symmetry.

In forthcoming sections, we discuss the resolutions of the equations (3.19), for quivers 1 and 2, discussed in Section 2.1. Before that, it is useful to discuss the *proper momentum*, which generalises that of [11]. We propose that the rate of change of the complexity is proportional to this *generalised proper momentum* in analogy with eq.(3.6).

3.2 Generalised proper momentum

We start defining the usual canonical momenta, as derivatives of the Lagrangian density with respect to the generalised velocity. We have

$$\begin{aligned} P_r &= \frac{m f_1(\eta) \dot{r}}{\sqrt{f_1(\eta) (e^{-2r(t)} - \dot{r}^2) - f_2(\eta) \dot{\eta}^2 - f_3(\eta) \dot{\varphi}^2}}, \\ P_\eta &= \frac{m f_2(\eta) \dot{\eta}}{\sqrt{f_1(\eta) (e^{-2r(t)} - \dot{r}^2) - f_2(\eta) \dot{\eta}^2 - f_3(\eta) \dot{\varphi}^2}}, \\ P_\varphi &= \frac{m f_3(\eta) \dot{\varphi}}{\sqrt{f_1(\eta) (e^{-2r(t)} - \dot{r}^2) - f_2(\eta) \dot{\eta}^2 - f_3(\eta) \dot{\varphi}^2}}. \end{aligned} \quad (3.20)$$

We can use eq.(3.17) for $r(t)$ together with the Hamiltonian in eq.(3.14) to find

$$P_r = \frac{m t f_1(\eta)}{(e^{2r_{UV}} + t^2) \sqrt{\frac{e^{2r_{UV}}}{(e^{2r_{UV}} + t^2)^2} f_1(\eta) - f_2(\eta) \dot{\eta}^2 - f_3(\eta) \dot{\varphi}^2}} = Ht. \quad (3.21)$$

We also find,

$$P_\eta = \frac{mf_2(\eta)\dot{\eta}}{\sqrt{\frac{e^{2r_{UV}}}{(e^{2r_{UV}}+t^2)^2}f_1(\eta) - f_2(\eta)\dot{\eta}^2 - f_3(\eta)\dot{\varphi}^2}}, \quad (3.22)$$

$$P_\varphi = \frac{mf_3(\eta)\dot{\varphi}}{\sqrt{\frac{e^{2r_{UV}}}{(e^{2r_{UV}}+t^2)^2}f_1(\eta) - f_2(\eta)\dot{\eta}^2 - f_3(\eta)\dot{\varphi}^2}}. \quad (3.23)$$

The idea now is to define a ‘proper coordinate’ ρ , such that

$$d\rho^2 = f_1(\eta)dr^2 + f_2(\eta)d\eta^2 + f_3(\eta)d\varphi^2. \quad (3.24)$$

Following the treatment in [20, 43], we encounter the set of equalities,

$$\begin{aligned} \mathcal{C}^{-1} &\equiv \frac{d\rho}{dr} = \pm \sqrt{f_1(\eta) + f_2(\eta) \left(\frac{\dot{\eta}}{\dot{r}}\right)^2 + f_3(\eta) \left(\frac{\dot{\varphi}}{\dot{r}}\right)^2}, \\ \mathcal{A}^{-1} &\equiv \frac{d\rho}{d\eta} = \pm \sqrt{f_1(\eta) \left(\frac{\dot{r}}{\dot{\eta}}\right)^2 + f_2(\eta) + f_3(\eta) \left(\frac{\dot{\varphi}}{\dot{\eta}}\right)^2}, \\ \mathcal{B}^{-1} &\equiv \frac{d\rho}{d\varphi} = \pm \sqrt{f_1(\eta) \left(\frac{\dot{r}}{\dot{\varphi}}\right)^2 + f_2(\eta) \left(\frac{\dot{\eta}}{\dot{\varphi}}\right)^2 + f_3(\eta)}. \end{aligned} \quad (3.25)$$

With these, the *generalised proper momentum* is

$$P_\rho = P_r \frac{\partial \dot{r}}{\partial \dot{\rho}} + P_\eta \frac{\partial \dot{\eta}}{\partial \dot{\rho}} + P_\varphi \frac{\partial \dot{\varphi}}{\partial \dot{\rho}} = \mathcal{C}P_r + \mathcal{A}P_\eta + \mathcal{B}P_\varphi = \sqrt{\frac{H^2(e^{2r_{UV}} + t^2)}{f_1(\eta(t))}} - 1. \quad (3.26)$$

In other words, the proper momentum receives a contribution from the usual canonical momentum along the radial direction, but also contributions from motion ‘across the quiver’, represented by $\mathcal{A}P_\eta$ and the motion in the R-symmetry direction given by $\mathcal{B}P_\varphi$. The evolution preserves the Hamiltonian H in eq.(3.14) and the R-charge J in eq.(3.15). Another way of expressing this is that the operator that spreads across the Hilbert space (as indicated at the beginning of this section), can have conserved quantum numbers (like an R-charge) and also explore different nodes in the quiver (which are connected by bifundamental fields).

It is important to mention that the signs in eq.(3.25) should be chosen appropriately according to the direction of motion along the geodesic. For instance, if a particle is falling from $r_{UV} \sim -\infty$ towards larger values of the r coordinate, while in ρ coordinate the motion is mapped to a trajectory from $\rho_{UV} \sim +\infty$ to smaller values of ρ , a minus sign should be chosen for the first relation in eq.(3.25). For η and φ directions, the same applies. In all cases, the last relation in eq. (3.26) remains valid and does not need further adjustments.

Finally, we *propose* that the relation with the rate of change of the complexity is that in eq.(3.6), but using the generalised proper momentum. Namely

$$\dot{C}(t) \sim P_\rho. \quad (3.27)$$

In what follows, we solve the equations of motion (3.19) for the quivers 1 and 2 in Section 2.1, as case studies. We need to resort to numerical study, which otherwise is simple. We

study first the two quivers in the case of zero angular momentum $J = 0$ (this is the operator that spreads has zero R-charge). This allows us to understand how the operator spreads across the quiver direction (an operator made out of bifundamental fields, it will spread across different nodes). After this, we discuss the effect of adding angular momentum (R-charge, $J \neq 0$) to this dynamics.

3.3 Geodesics with $J = 0$

In this section, we study the motion of the particle for the case of zero angular momentum $J = 0$. We make generic choices of initial position $\eta_0 \equiv \eta(t = 0)$ along with vanishing initial velocity in the quiver direction $\dot{\eta}(t = 0) = 0$. To have non-trivial η -dynamics, we must choose η_0 such that $f_1'(\eta = \eta_0) \neq 0$, as can be seen from equation (3.12). Recall that $J \sim \dot{\varphi} = 0$ is assumed in this section.

For this case, the Hamiltonian in equation (3.14) simplifies to,

$$H = \frac{m\sqrt{f_1(\eta_0)}}{e^{r_{UV}}}. \quad (3.28)$$

Substituting this expression in the second equation of (3.19), one gets

$$\dot{\eta} = \pm \frac{e^{r_{UV}}}{t^2 + e^{2r_{UV}}} \sqrt{\frac{f_1(\eta)}{f_2(\eta)} \left(1 - \frac{f_1(\eta)}{f_1(\eta_0)}\right)}, \quad (3.29)$$

which is consistent with the choice of initial conditions. Eq.(3.29) implies

$$f_1(\eta_0) \geq f_1(\eta(t)). \quad (3.30)$$

Additionally, eq.(3.29) allows solutions with negative and positive velocity. The sign of the velocity is fixed by the choice of initial position in the η -coordinate. By means of eq.(3.12), it is possible to understand how the sign is fixed by treating $f_1(\eta)$ as a potential term. An interesting feature is that, for both of the quivers, the function $f_1(\eta)$ has a global maximum located at η_{\max} (see Figure 2). As a consequence, the point $\eta = \eta_{\max}$ acts as an equilibrium position for the particle, meaning that if the particle starts at $\eta_0 = \eta_{\max}$, it remains there. For the two examples discussed in this paper, it is possible to compute η_{\max} in terms of the quiver parameters.

From a field theory perspective, this indicates that if the operator starts localised at a specific gauge node of the quiver (associated with η_{\max}), it will not spread to the rest of the nodes.

Since the quiver is of finite size (the η coordinate has a finite range), the particle may reach the ends of the η -space. In these cases, the particle *bounces* back elastically, changing the sign of the velocity $\dot{\eta}(t_*) \rightarrow -\dot{\eta}(t_*)$. Here, t_* is the time for which the particle reaches the end of the η -coordinate. Note that this sign change is allowed by eq. (3.29).

3.3.1 Quiver 1

For this first example, we consider the quiver closed by a flavour node, described by the function $\alpha_1(\eta)$. See Section 2.1.1 for details.

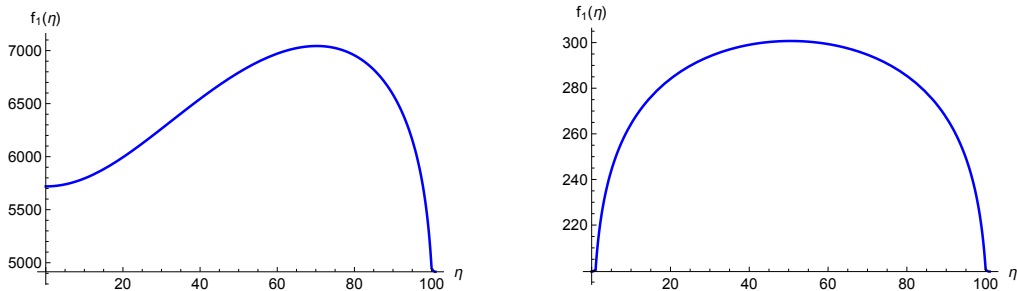


Figure 2. Plot of $f_1(\eta)$ for both quiver 1 (left) and quiver 2 (right). We set $P = 100$.

The full numerical solution for $\eta(t)$ is shown in Figures 3 and 5. For the first case, the particle moves towards decreasing values of η until it reaches the end of the space (at $\eta = 0$ or at $\eta = P + 1$), from which it bounces back and quickly stabilises. The motion on η is damped as the Figures 3 and 5 show. The contributions to the proper momentum from the η -momentum P_η , are relevant at early times (see Figure 4). On the other hand, for large t , equation (3.26) becomes

$$P_\rho(t) \Big|_{t \rightarrow \infty} = Ht = P_r, \quad (3.31)$$

meaning that for large times, the motion along the radial direction of AdS dominates the dynamics. This is in agreement with the linear growth of complexity and the fact that the dual theory is conformal.

The second case is depicted in Figures 5 and 6. Here, we consider a particle starting in the first branch of the quiver (for $0 \leq \eta \leq P$) and near the final gauge node of the quiver. In this case, the particle moves towards increasing η , reaching the final gauge node located at $\eta = P$. Then, it continues to the second branch of the quiver ($P \leq \eta \leq P + 1$) towards the flavour node at $\eta = P + 1$. Finally, the particle returns by changing the sign of the η -velocity in eq.(3.29) and returning to the first branch of the quiver. Despite the change in the direction of motion in η , the motion is still damped. Figure 6 shows that the contribution of the η motion to the proper momentum, is still localised at early times, in agreement with equation (3.31).

3.3.2 Quiver 2

In this example, we study the quiver in Section 2.1.2. This has two flavour nodes, at the beginning and at the end of the quiver, with constant rank gauge nodes. This is holographically described by the function $\alpha_2(\eta)$.

The first trajectory we study is shown in Figure 7. The particle starts at the second branch of the quiver ($1 \leq \eta \leq P$), quickly moves towards decreasing η , and changes to the first branch ($0 \leq \eta \leq 1$) followed by a bounce when reaching $\eta = 0$. After this, it bounces back on the first branch in the opposite direction, reaching the second branch, where it stops. The η -momentum of the particle is shown in Figure 8. The behavior is analogous to the one discussed in the previous example: at large times, the behavior is a generic

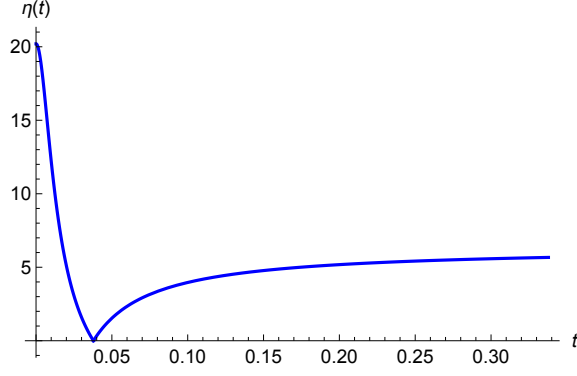


Figure 3. Trajectory of the particle in η for quiver 1. We set $J = 0$, $\eta_0 = 20$, $P = 100$ and $e^{r_{UV}} = 0.01$.

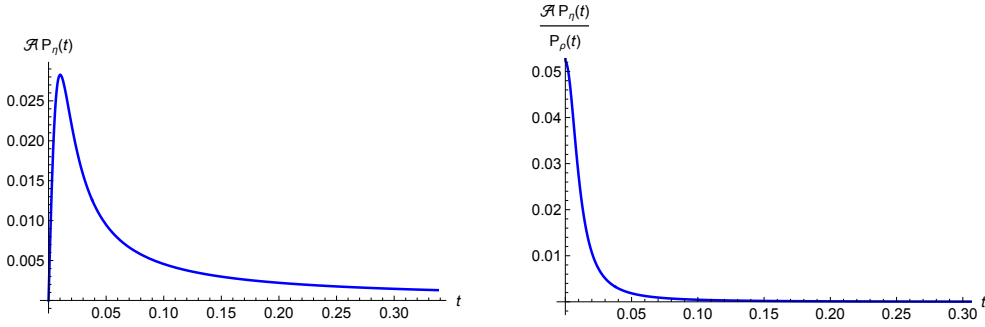


Figure 4. Momentum of the particle along the η direction (left) and contribution of the η momentum to the proper radial momentum. We set $J = 0$, $\eta_0 = 20$, $P = 100$ and $e^{r_{UV}} = 0.01$.

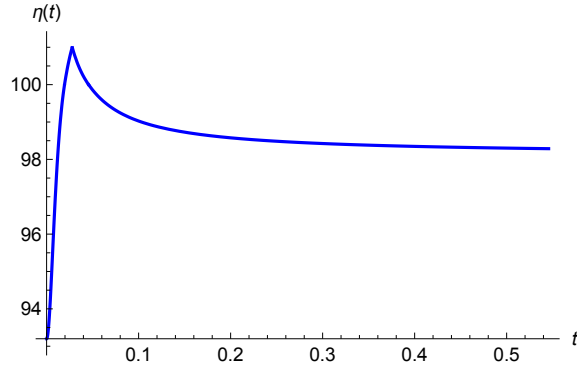


Figure 5. Trajectory of the particle in η for quiver 1. We set $J = 0$, $\eta_0 = 93$, $P = 100$ and $e^{r_{UV}} = 0.01$.

CFT—see eq.(3.31).

The second case study is shown in Figures 9 and 10, unlike the previous cases, the initial position of the particle is chosen such that the particle explores the middle section of the quiver without reaching the end-points. In this case, the particle goes toward increasing η , and explores only the second branch of the quiver, meaning $1 \leq \eta(t) \leq P$, quickly stopping

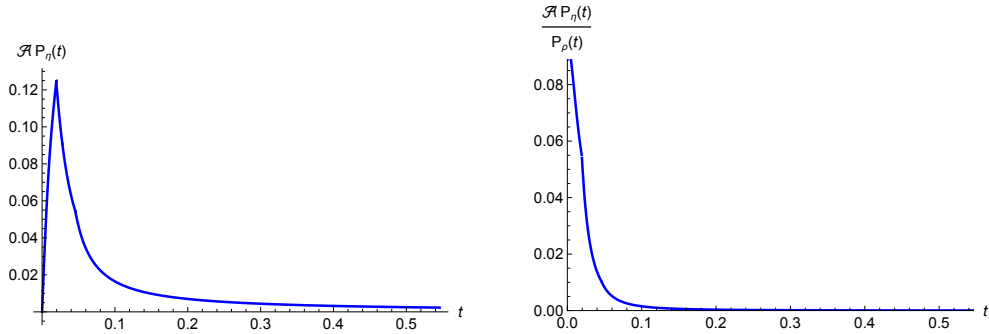


Figure 6. Momentum of the particle along the η direction (left) and contribution of the η momentum to the proper radial momentum. We set $J = 0$, $\eta_0 = 93$, $P = 100$ and $e^{r_{UV}} = 0.01$.

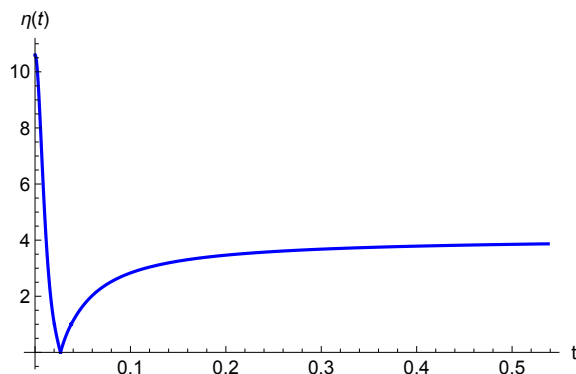


Figure 7. Trajectory of the particle in η for quiver 2. We set $J = 0$, $\eta_0 = 10$, $P = 100$ and $e^{r_{UV}} = 0.01$.

at a neighboring gauge node. Overall, the behavior agrees with equation (3.31) at large times, as both of the quivers describe CFTs.

Summary: this section was devoted to the study of geodesics with zero angular momentum $J = 0$, and how the particle explores the quiver direction by choosing different initial positions. One important aspect to focus on is the existence of an equilibrium position. From a dual field theory perspective, the CFT operator does not spread along the quiver. Moreover, we also highlight the CFT behavior at large times, which agrees with the late quadratic growth of the complexity.

3.4 Geodesics with $J \neq 0$

In this section, we study the motion of the particle for the case of non-zero angular momentum $J \neq 0$. We make generic choices of initial position $\eta_0 \equiv \eta(t = 0)$ along with zero initial velocity in the quiver direction $\dot{\eta}(t = 0) \equiv \dot{\eta}_0 = 0$, but with $\dot{\varphi}(t = 0) \equiv \dot{\varphi}_0 \neq 0$.

The equations of motion to be solved are those in (3.19), which we quote here to ease

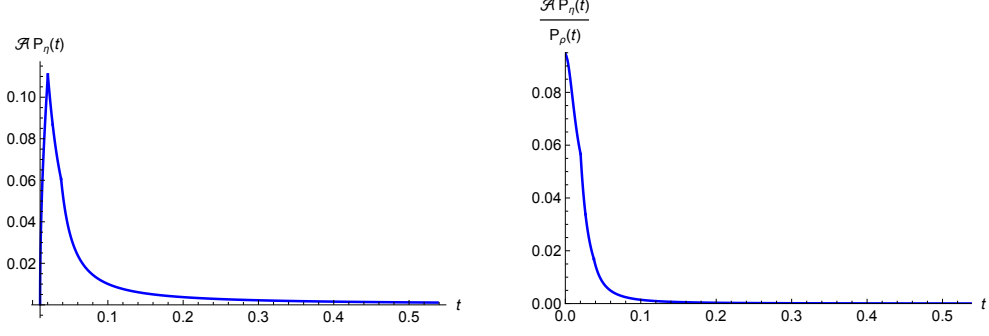


Figure 8. Momentum of the particle along the η direction (left) and contribution of the η momentum to the proper radial momentum. We set $J = 0$, $\eta_0 = 10$, $P = 100$ and $e^{r_{UV}} = 0.01$.

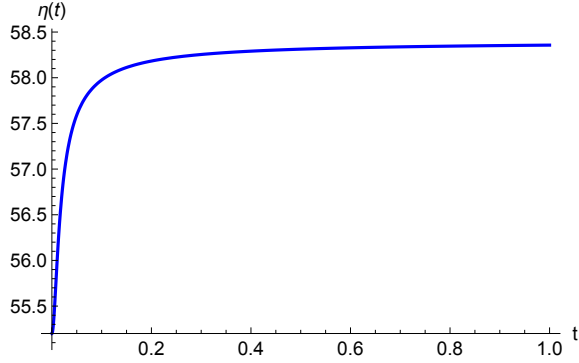


Figure 9. Trajectory of the particle in η for quiver 2. We set $J = 0$, $\eta_0 = 55$, $P = 100$ and $e^{r_{UV}} = 0.01$.

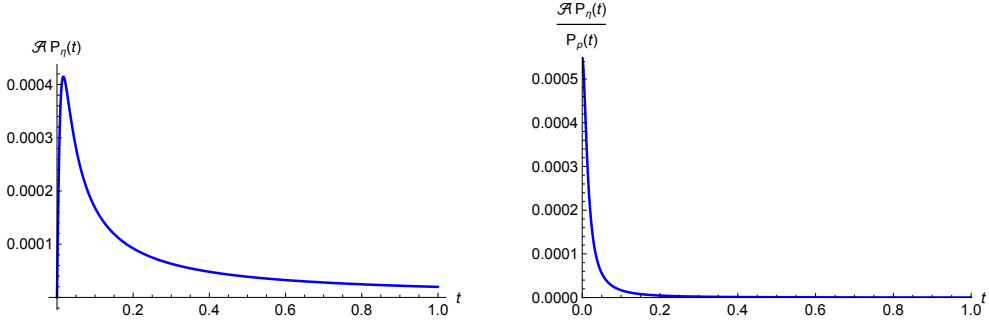


Figure 10. Momentum of the particle along the η direction (left) and contribution of the η momentum to the proper radial momentum for quiver 2. We set $J = 0$, $\eta_0 = 55$, $P = 100$ and $e^{r_{UV}} = 0.01$.

the reading,

$$\dot{\varphi} = \frac{J f_1(\eta)}{H f_3(\eta)} \left(\frac{1}{t^2 + e^{2r_{UV}}} \right), \quad (3.32)$$

$$\dot{\eta} = \pm \frac{1}{H} \left(\frac{1}{e^{2r_{UV}} + t^2} \right) \sqrt{\frac{f_1(\eta)}{f_2(\eta) f_3(\eta)} [H^2 e^{2r_{UV}} f_3(\eta) - m^2 f_1(\eta) (J^2 + f_3(\eta))]} \quad (3.33)$$

For this case, the Hamiltonian in eq. (3.14) and the angular momentum in eq. (3.15) simplify to

$$H = \frac{mf_1(\eta_0)e^{-2r_{UV}}}{\sqrt{f_1(\eta_0)(e^{-2r_{UV}}) - f_3(\eta_0)\dot{\varphi}_0^2}}. \quad (3.34)$$

$$J = \frac{f_3(\eta_0)}{\sqrt{f_1(\eta_0)(e^{-2r_{UV}}) - f_3(\eta_0)\dot{\varphi}_0^2}}\dot{\varphi}_0. \quad (3.35)$$

After using constraints in eqs. (3.34)-(3.35), analyzing eq. (3.33) shows that the function under the square root has one real root corresponding to the (r_{UV}, η_0) initial position and may have other real roots which restrict the range of the motion in some cases. This is due to the conservation of angular momentum, which is analysed on a case-by-case basis as follows in the next subsections.

As mentioned, in calculating the components of the generalised proper momenta defined in Section 3.2 as,

$$P_\rho = P_r \frac{\partial \dot{r}}{\partial \dot{\rho}} + P_\eta \frac{\partial \dot{\eta}}{\partial \dot{\rho}} + P_\varphi \frac{\partial \dot{\varphi}}{\partial \dot{\rho}} = \mathcal{C}P_r + \mathcal{A}P_\eta + \mathcal{B}P_\varphi = \sqrt{\frac{H^2(e^{2r_{UV}} + t^2)}{f_1(\eta(t))} - 1}, \quad (3.36)$$

we should be cautious regarding the signs appearing in the following equations

$$\mathcal{C}^{-1} \equiv \frac{d\rho}{dr} = \pm \sqrt{f_1(\eta) + f_2(\eta) \left(\frac{\dot{\eta}}{\dot{r}}\right)^2 + f_3(\eta) \left(\frac{\dot{\varphi}}{\dot{r}}\right)^2}, \quad (3.37)$$

$$\mathcal{A}^{-1} \equiv \frac{d\rho}{d\eta} = \pm \sqrt{f_1(\eta) \left(\frac{\dot{r}}{\dot{\eta}}\right)^2 + f_2(\eta) + f_3(\eta) \left(\frac{\dot{\varphi}}{\dot{\eta}}\right)^2}, \quad (3.38)$$

$$\mathcal{B}^{-1} \equiv \frac{d\rho}{d\varphi} = \pm \sqrt{f_1(\eta) \left(\frac{\dot{r}}{\dot{\varphi}}\right)^2 + f_2(\eta) \left(\frac{\dot{\eta}}{\dot{\varphi}}\right)^2 + f_3(\eta)}. \quad (3.39)$$

In our analysis, the value of the ρ coordinate is always decreasing from ρ_{UV} to smaller values. On the other hand, r increases from r_{UV} to larger values and φ increases from zero to larger values. Hence, a negative sign should be picked for the eq. (3.37) while eq. (3.39) carries only a plus sign. For the η direction, the sign should be chosen depending on the direction of motion.

In particular, if a bounce happens, this causes the particle to change the direction of motion, and then the sign changes. In all cases, the last relation in eq. (3.36) remains valid and does not need further adjustments.

Let us now discuss the numerical results for the quivers 1 and 2 in Section 2.1.

3.4.1 Quiver 1

As the first example, we consider the quiver closed by a flavour node, described by the function $\alpha_1(\eta)$ defined in Section 2.1.1.

The full numerical solution for $\eta(t)$ is shown in Figures 11 and 12. In the first case, the particle moves towards decreasing values of η , but contrary to the $J = 0$ case, it does not reach the end of the space (at $\eta = 0$). It bounces back from a certain value of η and quickly stabilises. This is due to the conservation of angular momentum, preventing the particle

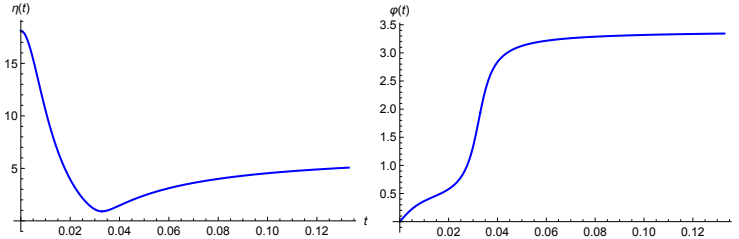


Figure 11. Trajectory of the particle in η (left) and φ (right) directions for Quiver 1 with $\eta_0 = 18$, $J = 0.0125$, $\dot{\varphi}_0 = 50$, $P = 100$ and $e^{r_{UV}} = 0.01$.

from reaching the end of space. It is clear from Figure 11 that the momentum P_φ (which is proportional to $\dot{\varphi}$) increases as the particle approaches the turning point. At the same time, $\dot{\eta}$ is decreasing. The increase in the angular φ momentum contributes in such a way that the constraints from the Hamiltonian and total angular momentum J are satisfied. After the bounce, the momentum in the η direction increases again and takes over while angular rotation almost stops — see first two panels in Figure 12. In other words, the particle can not reach $\eta = 0$ otherwise the momentum in φ direction would diverge.

The motions on the η and φ directions are damped as Figure 11 shows. The contributions to the proper momentum coming from P_η and that coming from P_φ , are relevant at early times (see the last panel of Figure 12). On the other hand, for large t , equation (3.26) approximates

$$P_\rho(t) \Big|_{t \rightarrow \infty} = Ht = P_r, \quad (3.40)$$

This means that for late times, the motion along the radial direction of AdS dominates the dynamics. This is in agreement with the linear growth of complexity and the fact that the dual theory is conformal. We do not plot $P_\rho(t)$ for these examples as the behavior is linear and similar at the late times.

A second situation is depicted in Figure 13. Here, the particle starts in the first branch of the quiver (for $0 \leq \eta \leq P$) and near the final gauge node of the quiver. The particle moves towards increasing η , asymptotically reaching the final gauge node located at $\eta = P$. The motion is damped, and it does not reach the second branch of the quiver ($P \leq \eta \leq P + 1$). The contribution of the motion in η and φ directions to the proper momentum is still mostly localised at early times, in agreement with equation (3.40). Let us now study the complexity for the second quiver.

3.4.2 Quiver 2

We study the quiver in Section 2.1.2. This has two flavour nodes, at the beginning and at the end of the quiver, with constant rank gauge nodes. This information is encoded in the function $\alpha_2(\eta)$.

The first trajectory we study is shown in Figure 14. The particle starts at the second branch of the quiver ($1 \leq \eta \leq P$), quickly moves towards decreasing η , and changes to the first branch ($0 \leq \eta \leq 1$), but it does not reach $\eta = 0$ and continues in the first branch

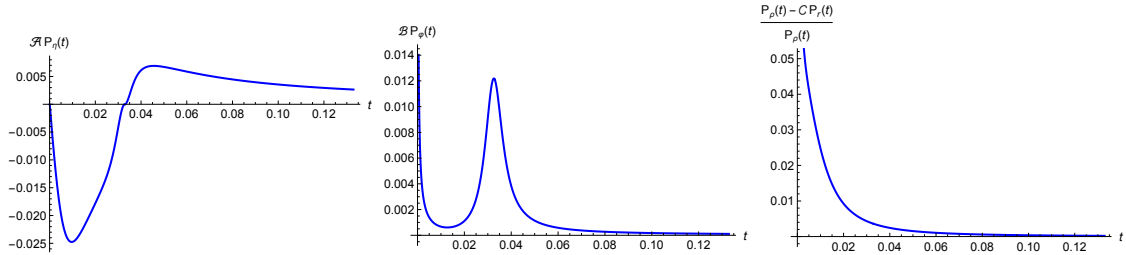


Figure 12. The components of the particle momentum in η (left) and φ (middle) directions and $(P_\rho - CP_r)/P_\rho$ (right) for Quiver 1 with $\eta_0 = 18$, $J = 0.0125$, $\dot{\varphi}_0 = 50$, $P = 100$ and $e^{r_{UV}} = 0.01$.

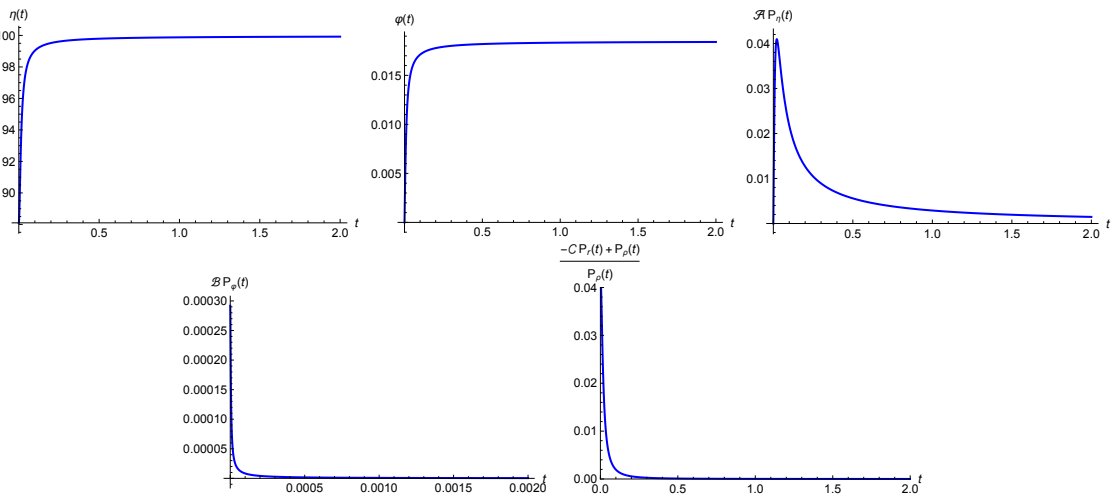


Figure 13. Trajectory of the particle in η and φ directions, the components of the particle momentum in η and φ directions and $(P_\rho - CP_r)/P_\rho$ for Quiver 1 with $\eta_0 = 88$, $J = 6.67 \times 10^{-5}$, $\dot{\varphi}_0 = 1.1$, $P = 100$ and $e^{r_{UV}} = 0.01$.

where it stops. This should be compared with the similar study in Section 3.3.2 with zero J as the particle bounces there. The η and φ -momenta of the particle are shown in Figure 15. The behavior is analogous to the one discussed in the previous example, as at large times it resembles the one found in a generic CFT, see eq.(3.31).

In summary: in this section, we studied the geodesics of a particle falling in our background with non-zero angular momentum and different initial positions. The most important observation is that due to the existence of conserved charges (like J), the particle motion is non trivially affected. It can not approach the endpoints of the η direction and bounces back before reaching them. At late times, the momentum contribution coming from the radial direction P_r takes over the other contributions from P_η, P_φ . The bottom-up CFT behaviour [11] emerges, as it happens in the previously studied cases.

4 Discussion, Further Comments and Conclusions

In this work, we studied aspects of Krylov (spread) complexity for a class of six-dimensional $\mathcal{N} = (1, 0)$ superconformal field theories and their holographic duals in massive type IIA su-

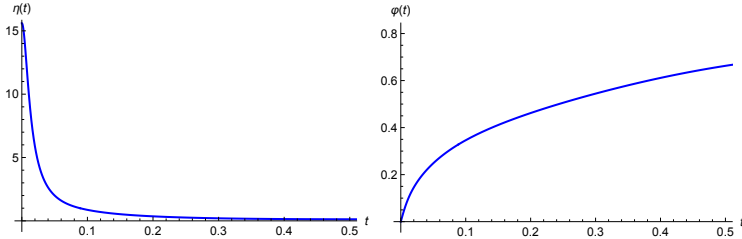


Figure 14. Trajectory of the particle in η (left) and ϕ (right) directions for Quiver 2 with $\eta_0 = 15$, $J \neq 0$, $\dot{\varphi}_0 = 10$, $P = 100$ and $e^{r_{UV}} = 0.01$.

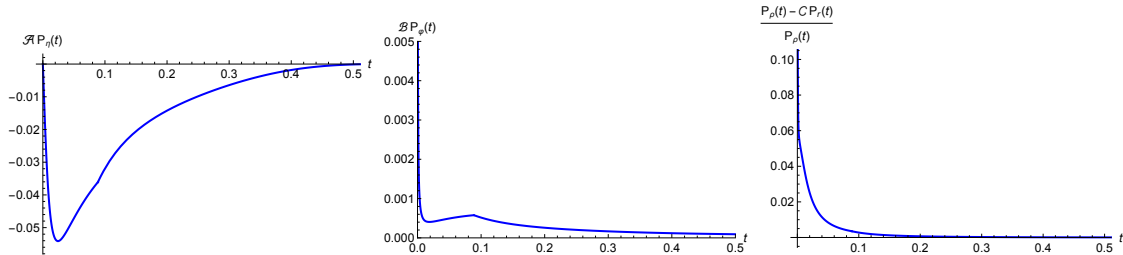


Figure 15. The components of the particle momentum in η (left) and φ (middle) directions and $(P_\varphi - CP_\varphi)/P_\varphi$ (right) for Quiver 2 with $\eta_0 = 15$, $J = 0.0001$, $\dot{\varphi}_0 = 10$, $P = 100$ and $e^{r_{UV}} = 0.01$.

pergravity. These theories are engineered by Hanany-Witten brane constructions involving NS5, D6 and D8 branes and admit holographic descriptions in terms of AdS_7 backgrounds characterised by a function $\alpha(\eta)$ that encodes the data of the dual linear quiver. We reviewed this construction and presented two representative examples of quivers that we use as case studies. Building on recent proposals relating the growth rate of Krylov complexity to the proper momentum of an infalling particle in the bulk geometry, we extended this prescription to the AdS_7 backgrounds relevant for these six-dimensional theories.

Within this framework, the spreading of operators in the strongly coupled SCFT is modelled holographically by the motion of a massive particle following timelike geodesics in the bulk geometry. Motion along the internal S^2 directions encodes the presence of $SU(2)_R$ charge. This is in nice correspondence with symmetry resolved Krylov complexity [21, 22]. Motion along the coordinate η captures the possibility that the operator spreads across different nodes of the quiver. Solving the resulting equations of motion numerically for two illustrative quiver theories, both for vanishing and non-vanishing angular momentum, we found that the dynamics along the quiver direction is typically damped and largely restricted to early times, while at late times the motion is dominated by the AdS radial direction. As a consequence, the generalised proper momentum, and hence the rate of holographic complexity growth, approaches a linear behaviour at late times, consistent with expectations for conformal theories. These results provide a geometric picture for how operator spreading, global charges and quiver structure are encoded in the holographic description of complexity in higher-dimensional SCFTs.

Interestingly, one can make a comparison between the results with the non-zero angular momentum case studied here and similar results obtained in Ref. [43]. In both cases, the

proper momentum and complexity are altered considerably at early times, while in late time, the effect of the addition of angular momenta dual to the R-charge is less visible. It is noteworthy that in the case of this paper, late time behaviour of the complexity is dominated by that of CFTs. In contrast, for confining backgrounds [43, 44], it resembles the complexity growth in gapped systems [45].

There are several interesting directions in which the present work could be extended. A natural development would be to perform the field theory calculation of Krylov complexity directly in the six-dimensional SCFTs discussed here, allowing for a more precise comparison with the holographic predictions. It would also be interesting to explore more general quiver configurations and study how the structure of the rank function $R(\eta)$ influences the spreading of operators across the quiver. Another promising direction is to analyse related observables in these backgrounds, such as operator growth, chaos diagnostics [28, 46], entanglement or other measures of quantum information, in order to better understand the interplay between complexity, global symmetries and the structure of strongly coupled higher-dimensional field theories. Finally, it would be worthwhile to investigate whether similar constructions can be developed for other holographic systems, including theories with reduced supersymmetry or non-conformal dynamics, see for example in backgrounds like [47, 48, 48–54].

Acknowledgments:

Various colleagues have contributed to our understanding and the presentation of the material in this work. We thank: Nicolás Bragagnolo (also for collaborations!), Pawel Caputa, Dimitrios Chatzis, Madison Hammond, Horatiu Nastase, Alfonso Ramallo, Dibakar Roychowdhury, Dimitrios Zoakos. C. N. is supported by STFC’s grants ST/Y509644-1, ST/X000648/1 and ST/T000813/1. The work of R.T. has been supported by EPSRC Grant EP/Z535175/1 and STFC grant UKRI1787.

References

- [1] S. Baiguera, V. Balasubramanian, P. Caputa, S. Chapman, J. Haferkamp, M. P. Heller et al., *Quantum complexity in gravity, quantum field theory, and quantum information science*, [2503.10753](#).
- [2] E. Rabinovici, A. Sánchez-Garrido, R. Shir and J. Sonner, *Krylov Complexity*, [2507.06286](#).
- [3] P. Nandy, A. S. Matsoukas-Roubeas, P. Martínez-Azcona, A. Dymarsky and A. del Campo, *Quantum dynamics in Krylov space: Methods and applications*, *Phys. Rept.* **1125-1128** (2025) 1 [[2405.09628](#)].
- [4] J. M. Maldacena, *The Large N limit of superconformal field theories and supergravity*, *Adv. Theor. Math. Phys.* **2** (1998) 231 [[hep-th/9711200](#)].
- [5] D. E. Parker, X. Cao, A. Avdoshkin, T. Scaffidi and E. Altman, *A Universal Operator Growth Hypothesis*, *Phys. Rev. X* **9** (2019) 041017 [[1812.08657](#)].
- [6] E. Rabinovici, A. Sánchez-Garrido, R. Shir and J. Sonner, *A bulk manifestation of Krylov complexity*, *JHEP* **08** (2023) 213 [[2305.04355](#)].

- [7] P. Caputa, J. M. Magan and D. Patramanis, *Geometry of Krylov complexity*, *Phys. Rev. Res.* **4** (2022) 013041 [[2109.03824](#)].
- [8] P. Caputa and K. Kutak, *Krylov complexity and gluon cascades in the high energy limit*, *Phys. Rev. D* **110** (2024) 085011 [[2404.07657](#)].
- [9] A. Avdoshkin, A. Dymarsky and M. Smolkin, *Krylov complexity in quantum field theory, and beyond*, *JHEP* **06** (2024) 066 [[2212.14429](#)].
- [10] J. L. F. Barbón and M. Sasieta, *Holographic Bulk Reconstruction And Cosmological Singularities*, *JHEP* **09** (2019) 026 [[1906.04745](#)].
- [11] P. Caputa, B. Chen, R. W. McDonald, J. Simón and B. Strittmatter, *Spread Complexity Rate as Proper Momentum*, [2410.23334](#).
- [12] A. Hanany and E. Witten, *Type IIB superstrings, BPS monopoles, and three-dimensional gauge dynamics*, *Nucl. Phys. B* **492** (1997) 152 [[hep-th/9611230](#)].
- [13] A. Hanany and A. Zaffaroni, *Branes and six-dimensional supersymmetric theories*, *Nucl. Phys. B* **529** (1998) 180 [[hep-th/9712145](#)].
- [14] D. Gaiotto and A. Tomasiello, *Holography for (1,0) theories in six dimensions*, *JHEP* **12** (2014) 003 [[1404.0711](#)].
- [15] S. Cremonesi and A. Tomasiello, *6d holographic anomaly match as a continuum limit*, *JHEP* **05** (2016) 031 [[1512.02225](#)].
- [16] F. Apruzzi, M. Fazzi, D. Rosa and A. Tomasiello, *All AdS₇ solutions of type II supergravity*, *JHEP* **04** (2014) 064 [[1309.2949](#)].
- [17] F. Apruzzi, M. Fazzi, A. Passias, A. Rota and A. Tomasiello, *Six-Dimensional Superconformal Theories and their Compactifications from Type IIA Supergravity*, *Phys. Rev. Lett.* **115** (2015) 061601 [[1502.06616](#)].
- [18] A. Passias, A. Rota and A. Tomasiello, *Universal consistent truncation for 6d/7d gauge/gravity duals*, *JHEP* **10** (2015) 187 [[1506.05462](#)].
- [19] D. Chatzis, A. Fatemiabhari, M. Giliaberti and M. Hammond, *Holographic Entanglement Entropy in Quiver Theories*, [2509.19434](#).
- [20] A. Fatemiabhari, H. Nastase, C. Nunez and D. Roychowdhury, *Holographic Krylov Complexity for Conformal Quiver Gauge Theories*, [2512.14812](#).
- [21] P. Caputa, G. Di Giulio and T. Q. Loc, *Growth of block-diagonal operators and symmetry-resolved Krylov complexity*, *Phys. Rev. Res.* **7** (2025) 043055 [[2507.02033](#)].
- [22] P. Caputa, G. Di Giulio and T. Q. Loc, *Symmetry-Resolved Spread Complexity*, [2509.12992](#).
- [23] N. Seiberg, *Nontrivial fixed points of the renormalization group in six-dimensions*, *Phys. Lett. B* **390** (1997) 169 [[hep-th/9609161](#)].
- [24] U. H. Danielsson, G. Ferretti, J. Kalkkinen and P. Stjernberg, *Notes on supersymmetric gauge theories in five-dimensions and six-dimensions*, *Phys. Lett. B* **405** (1997) 265 [[hep-th/9703098](#)].
- [25] S. Cremonesi and A. Tomasiello, *6d holographic anomaly match as a continuum limit*, *Journal of High Energy Physics* **2016** (2015) 1.
- [26] C. Nunez, L. Santilli and K. Zarembo, *Linear Quivers at Large-N*, [2311.00024](#).

- [27] C. Núñez, J. M. Penín, D. Roychowdhury and J. Van Gersel, *The non-Integrability of Strings in Massive Type IIA and their Holographic duals*, *JHEP* **06** (2018) 078 [[1802.04269](#)].
- [28] K. Filippas, C. Núñez and J. Van Gersel, *Integrability and holographic aspects of six-dimensional $\mathcal{N} = (1, 0)$ superconformal field theories*, *JHEP* **06** (2019) 069 [[1901.08598](#)].
- [29] F. Apruzzi and M. Fazzi, *AdS₇/CFT₆ with orientifolds*, *JHEP* **01** (2018) 124 [[1712.03235](#)].
- [30] F. Apruzzi, N. Mekareeya, B. Robinson and A. Tomasiello, *New punctures for six-dimensional compactifications*, *JHEP* **02** (2026) 214 [[2510.17972](#)].
- [31] C. Nunez and D. Roychowdhury, *Time-like Entanglement Entropy: a top-down approach*, [2505.20388](#).
- [32] C. Nunez and D. Roychowdhury, *Interpolating between spacelike and timelike entanglement via holography*, *Phys. Rev. D* **112** (2025) L081902 [[2507.17805](#)].
- [33] C. Nunez and D. Roychowdhury, *Holographic timelike entanglement across dimensions*, *JHEP* **11** (2025) 100 [[2508.13266](#)].
- [34] N. Jokela, J. Kastikainen, C. Nunez, J. M. Penín, H. Ruotsalainen and J. G. Subils, *On entanglement c-functions in confining gauge field theories*, [2505.14397](#).
- [35] M. Giliberti, A. Fatemiabhari and C. Nunez, *Confinement and screening via holographic Wilson loops*, *JHEP* **11** (2024) 068 [[2409.04539](#)].
- [36] A. Conti, G. Dibitetto, Y. Lozano, N. Petri and A. Ramírez, *Deconstruction and surface defects in 6d CFTs*, *JHEP* **11** (2024) 131 [[2407.21627](#)].
- [37] F. Apruzzi, N. Mekareeya, B. Robinson and A. Tomasiello, *Superconformal anomalies for string defects in six-dimensional $\mathcal{N} = (1, 0)$ SCFTs*, *JHEP* **12** (2024) 153 [[2407.18049](#)].
- [38] M. Lima, *Spin-2 universal minimal solutions on type IIA and IIB supergravity*, *JHEP* **05** (2024) 303 [[2310.16536](#)].
- [39] O. Bergman, M. Fazzi, D. Rodríguez-Gómez and A. Tomasiello, *Charges and holography in 6d (1,0) theories*, *JHEP* **05** (2020) 138 [[2002.04036](#)].
- [40] E. Malek, H. Samtleben and V. Vall Camell, *Supersymmetric AdS₇ and AdS₆ vacua and their consistent truncations with vector multiplets*, *JHEP* **04** (2019) 088 [[1901.11039](#)].
- [41] P.-Z. He, *Revisit the relationship between spread complexity rate and radial momentum*, [2411.19172](#).
- [42] Z.-Y. Fan, *Momentum-Krylov complexity correspondence*, [2411.04492](#).
- [43] A. Fatemiabhari and C. Nunez, *Krylov Complexity, Confinement and Universality*, [2602.17757](#).
- [44] A. Fatemiabhari, H. Nastase, C. Nunez and D. Roychowdhury, *Holographic Krylov complexity in confining gauge theories*, [2511.22717](#).
- [45] X. Jiang, J. C. Halimeh and N. S. Srivatsa, *Krylov Complexity Meets Confinement*, *Phys. Rev. D* (2025) [[2511.03783](#)].
- [46] C. Núñez, D. Roychowdhury and D. C. Thompson, *Integrability and non-integrability in $\mathcal{N} = 2$ SCFTs and their holographic backgrounds*, *JHEP* **07** (2018) 044 [[1804.08621](#)].
- [47] A. Anabalón and S. F. Ross, *Supersymmetric solitons and a degeneracy of solutions in AdS/CFT*, *JHEP* **07** (2021) 015 [[2104.14572](#)].

- [48] A. Anabalón, A. Gallerati, S. Ross and M. Trigiante, *Supersymmetric solitons in gauged $\mathcal{N} = 8$ supergravity*, *JHEP* **02** (2023) 055 [[2210.06319](#)].
- [49] A. Anabalón, H. Nastase and M. Oyarzo, *Supersymmetric AdS Solitons and the interconnection of different vacua of $\mathcal{N} = 4$ Super Yang-Mills*, [2402.18482](#).
- [50] D. Chatzis, A. Fatemiabhari, C. Nunez and P. Weck, *SCFT deformations via uplifted solitons*, [2406.01685](#).
- [51] D. Chatzis, A. Fatemiabhari, C. Nunez and P. Weck, *Conformal to confining SQFTs from holography*, [2405.05563](#).
- [52] D. Chatzis, M. Hammond, G. Itsios, C. Nunez and D. Zoakos, *Universal Observables, SUSY RG-Flows and Holography*, [2506.10062](#).
- [53] D. Chatzis, M. Hammond, G. Itsios, C. Nunez and D. Zoakos, *Supersymmetric AdS Solitons, Coulomb Branch Flows and Twisted Compactifications*, [2511.18128](#).
- [54] A. Fatemiabhari and C. Nunez, *From conformal to confining field theories using holography*, *JHEP* **03** (2024) 160 [[2401.04158](#)].